

Molecular supersonic jet studies of aniline solvation by helium and methane

E. R. Bernstein, K. Law, and Mark Schauer

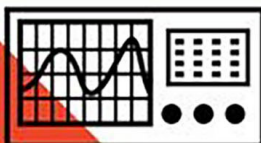
Citation: *The Journal of Chemical Physics* **80**, 634 (1984); doi: 10.1063/1.446774

View online: <http://dx.doi.org/10.1063/1.446774>

View Table of Contents: <http://aip.scitation.org/toc/jcp/80/2>

Published by the *American Institute of Physics*

**COMPLETELY
REDESIGNED!**



**PHYSICS
TODAY**

Physics Today Buyer's Guide
Search with a purpose.

Molecular supersonic jet studies of aniline solvation by helium and methane^{a)}

E. R. Bernstein, K. Law, and Mark Schauer

Department of Chemistry, Condensed Matter Sciences Laboratory, Colorado State University, Fort Collins, Colorado 80523

(Received 31 August 1983; accepted 6 October 1983)

The technique of two color resonant two photon ionization coupled with time of flight mass spectroscopy has been employed to study aniline-He (AnHe_x) and aniline- CH_4 [$\text{An}(\text{CH}_4)_x$] van der Waals clusters generated in a supersonic molecular jet. This technique allows identification of spectroscopic transitions with clusters of known mass because no ion fragmentation is observed. Specific features in the optical fluorescence excitation and dispersed emission spectra can thereby be uniquely identified with a particular cluster. Cluster vibrations can be analyzed by a Morse potential to yield the An-He bond dissociation energy $D_0 \sim 100 \pm 50 \text{ cm}^{-1}$. Careful analysis of the dispersed emission from AnHe_x suggests $145 < D_0 < 155 \text{ cm}^{-1}$. It is found that the van der Waals bond stretching frequency is nearly the same in the ground and excited states and that there is a strong propensity rule for $\Delta V = 0$ ($V = \text{vdW}$ bond mode) as expected in this case, although $\Delta V = \pm 1$ transitions can be observed. The AnHe_1 and AnHe_2 origins are slightly red shifted with respect to the An origins, while the AnHe_x ($x \geq 3$) origin is broad and nearly unshifted. This pattern is followed for $\text{An}(\text{CH}_4)_x$ clusters; AnCH_4 transitions are red shifted 80 cm^{-1} from the comparable An features and $\text{An}(\text{CH}_4)_2$ transitions are 160 cm^{-1} below their comparable An feature. The $\text{An}(\text{CH}_4)_x$ ($x \geq 3$) transitions appear at $\sim 200\text{--}300 \text{ cm}^{-1}$ below their comparable An mode. The binding energy for the An- CH_4 bond is found to be $500 < D_0 < 700 \text{ cm}^{-1}$ in the 1B_2 state of aniline. Aniline has a strong preference for binding the solvent above and below the aromatic ring. Since the D_0 is large for An- CH_4 and the stretching mode is only $\sim 25 \text{ cm}^{-1}$ the $\text{An}(\text{CH}_4)_x$ system builds up a large density of states in the van der Waals degrees of freedom. This density of states allows intramolecular vibrational redistribution (IVR) to take place, if the An mode excited is lower in energy than the D_0 value. The rate of IVR from $6a^1$ ($O_0^0 + 500 \text{ cm}^{-1}$) is somewhat faster than the 5 ns fluorescence rate but much slower than the rate of vibrational predissociation (VP) from higher levels. Both the IVR process, due to the van der Waals vibrational density of states, and the limiting solvent red shift, at a value similar to that found for cryogenic solutions, are discussed in terms of these clusters as model solute/solvent systems.

I. INTRODUCTION

It is well known that the supersonic molecular jet is a powerful tool for generating and studying weakly bound van der Waals (vdW) clusters.¹ Clusters formed between a large central molecule and one or more carrier gas species can be thought of as a microscopic solution. The solvation of the seeded molecule can be monitored spectroscopically as experimental parameters such as nozzle backing pressure (P_0), nozzle diameter, and concentration of solvent species are varied.² However, often the stoichiometry of the cold cluster generated in the beam cannot be unambiguously determined by optical techniques. Monitoring the intensity of certain spectral features as P_0 is changed can identify the particular feature as a cluster related transition,³ but these studies are not always definitive for stoichiometry, especially in cases for which congestion in the spectral region is substantial.

Experiments using mass spectroscopy can give information about cluster size. However, electron impact or one-color multiphoton ionization techniques can impart excess energy to the cluster and cause fragmentation.⁴ The technique of two-color resonant two-photon ionization time-of-flight mass spectroscopy (two-color MS) can be used to ionize the clusters without fragmentation.⁵ Using this technique, it is possible to ob-

tain absorption spectra of an unambiguously mass-identified vdW cluster. Thus, the two-color MS experiment greatly enhances the ability to interpret fluorescence excitation (FE) and dispersed emission (DE) spectra obtained from species generated in the beam.

In a previous publication, hereafter referred to as I,⁶ we have addressed the relaxation mechanisms of aniline (An) and aniline-helium (AnHe_x) in the jet, as well as various spectroscopic properties of the AnHe_x clusters. The two-color MS studies reported in the present paper contribute to a better understanding of AnHe_x clusters with regard to relaxation processes and energy levels.

Several aspects of the An- CH_4 system have also been explored. These studies emphasize that two-color MS experiments are essential to the study of vdW clusters and that they complement the FE and DE techniques. The two-color MS experiment can be used to identify the origins and vdW vibrations associated with $\text{An}(\text{CH}_4)$ and $\text{An}(\text{CH}_4)_2$ vibronic transitions. With this information it is possible to assign several cluster DE spectra.

The Results and Discussion sections of this paper are each divided into two parts. First, new information concerning the An-He system will be presented and discussed. Next, the results of FE, DE, and two-color MS studies of the An- CH_4 system will be presented; then the similarities and differences between the An-He and An- CH_4 systems will be addressed.

^{a)}Supported in part by a grant from ARO-D and ONR.

II. EXPERIMENTAL PROCEDURES

The molecular jet apparatus and procedures for obtaining FE and DE spectra have been described in detail in I. Beam conditions and laser powers are the same as described in I except for changes in P_0 as indicated in the figure captions. Laser power levels for DE, FE, and TOFMS experiments were always maintained below saturation limits. The procedures for obtaining one-color and two-color MS data will be presented here.

Both one-color and two-color resonance enhanced, two photon ionization, time-of-flight mass spectra were obtained for the An-He and An-CH₄ systems. Two color mass spectroscopy can provide information on van der Waals clusters which is not readily attainable through one-color MS studies. For aniline, the absorption of the second photon in a one-color MS experiment provides $\sim 7000 \text{ cm}^{-1}$ of excess vibration energy to a cluster ion which causes substantial fragmentation of the ion. Two-color MS experiments require two laser beams, the first excites the species of interest to its first excited state (ν_{pump}), and the second beam excites the species to create the ion (ν_{ion}). These two beams are supplied by two Nd:YAG pumped dye laser systems (Quanta Ray). The two lasers are synchronized by triggering one from the other and relative jitter in the light pulses is $\leq 5 \text{ ns}$ as measured by a 1P28 phototube. The ionization thresholds of An, AnHe_x, and An(CH₄)_x at various vibronic levels are determined by scanning ν_{ion} while keeping ν_{pump} constant. The pump beam intensity is reduced to the point at which no signal is observed without ν_{ion} . These procedures assure that very little fragmentation of the vdW clusters occurs.

Experimental conditions for obtaining the spectra are described in the figure captions. The peaks in the DE spectra are slit width limited at $\sim 15 \text{ cm}^{-1}$ unless otherwise stated. FE, one-color, and two-color MS line-widths are only limited by the frequency width of the lasers $\sim 0.25 \text{ cm}^{-1}$. The spectra are calibrated using the opto-galvanic effect with an Fe-Ne hollow cathode lamp.⁷

The optimum concentration of solvent is determined by maximizing the absorption signal of the desired species observed through the particular detection technique being used (e.g., FE, two-color MS). The error in the quoted concentrations of solvent is less than 5%. The solute trap is not heated and the concentration of solute varies with P_0 . Research grade methane and aniline, and commercial grade helium are used.

III. RESULTS

A. An-He system

As pointed out in the last section, much less fragmentation of vdW species is observed in the two-color than in the one-color MS experiment. This is readily seen by comparing Fig. 1 and Fig. 2. In one-color MS (Fig. 1) absorption features due to AnHe and AnHe₂ are present in the absorption spectrum taken while gating on the An mass channel. Also, absorption features due

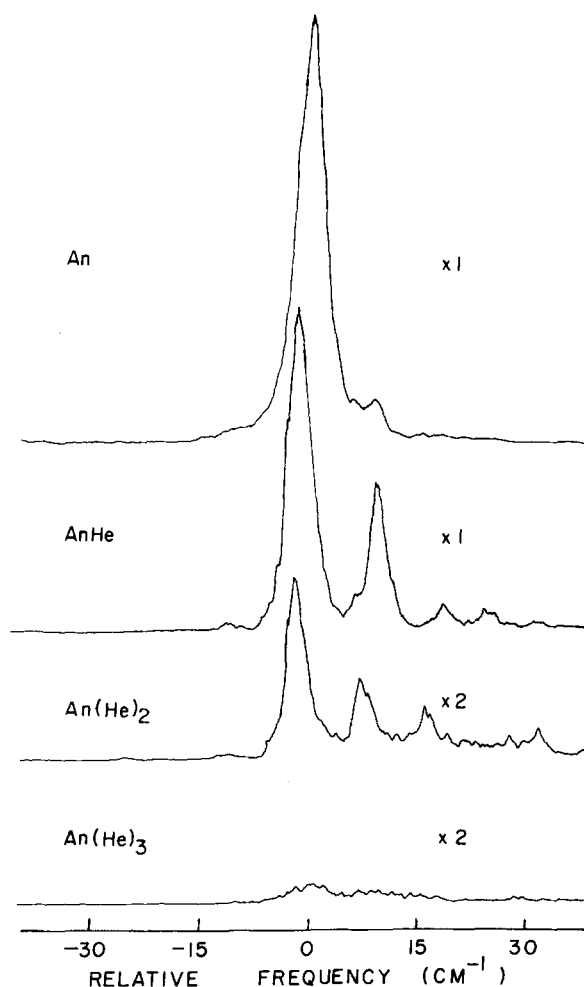


FIG. 1. One color mass spectra obtained by grating on the labeled mass channel. An was expanded in pure He at 600 psi backing pressure. The frequency scale is relative to An 0_0^0 . Fragmentation of clusters due to creating ions with excess vibrational energy causes absorption due to high clusters to appear in the An and AnHe spectra.

to AnHe₂ appear in the AnHe spectrum. While the one-color MS are distorted by fragmentation, they are more intense than the corresponding two-color spectra; it thus is possible to obtain one-color mass spectra, but not two-color mass spectra, of the AnHe₃ species as the AnHe₃ peaks are considerably broader and weaker than the smaller cluster peaks. Also, the shift of the AnHe₃ 0_0^0 relative to the An 0_0^0 is different than would be predicted based on the AnHe and AnHe₂ spectral shifts. It appears that the third He may attach to a different position on the An than the first two.

The two-color mass spectra show clearly the undistorted spectra of An, AnHe, and AnHe₂ in the region of the An 0_0^0 (Fig. 2). These spectra show an additive red shift of the 0_0^0 transition upon addition of one and two He, and a progression in the An-He stretch (see Table I). From the An-He stretching frequency and anharmonicity, it is possible to estimate the binding energy for the cluster (based on an assumed Morse potential) as $100 \pm 50 \text{ cm}^{-1}$. This calculation is very crude, not only because a Morse potential was assumed, but

TABLE I. van der Waals modes (in relative cm^{-1}) for $\text{AnHe}_x 0_0^0$ as determined by two-color MS experiments (Fig. 2). $\text{AnHe} 0_0^0$ and $\text{AnHe}_2 0_0^0$ are red shifted from $\text{An} 0_0^0$ by 1.1 and 1.9 cm^{-1} , respectively.

	v^1	v^2	v^3
AnHe	10.4	19.7	28.5
AnHe ₂	9.2	17.3	25.2

because small errors in the peak positions of the weakest peaks can lead to large errors in the calculated binding energy. Better estimates are available from the DE data which will be elaborated upon in the Discussion section.

The assignment of the AnHe and AnHe₂ two-color MS as consisting of a red shifted origin and vdW stretches to the blue is supported by the high resolution DE spectra shown in Fig. 3. As the 0_0^0 of AnHe (and necessarily An and AnHe₂) is pumped, the DE spectrum shows at least one member of a progression of the vdW stretch in the ground state. The transition shown is I_2^0

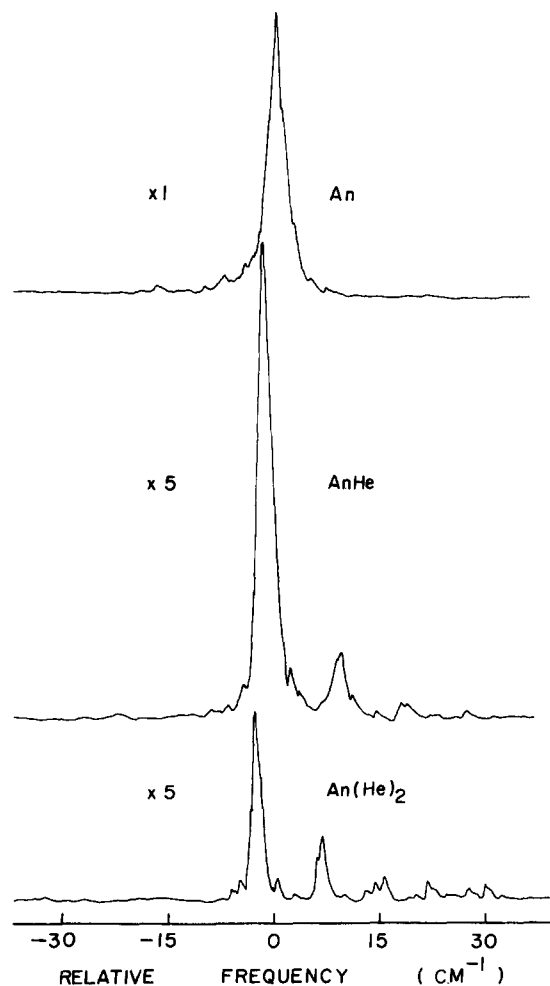


FIG. 2. Two-color MS gated on the labeled species. An was expanded in pure He at $P_0 = 600$ psi. The frequency scale is relative to $\text{An} 0_0^0$. Note that fragmentation has been virtually eliminated. The ionization frequency is 28169 cm^{-1} .

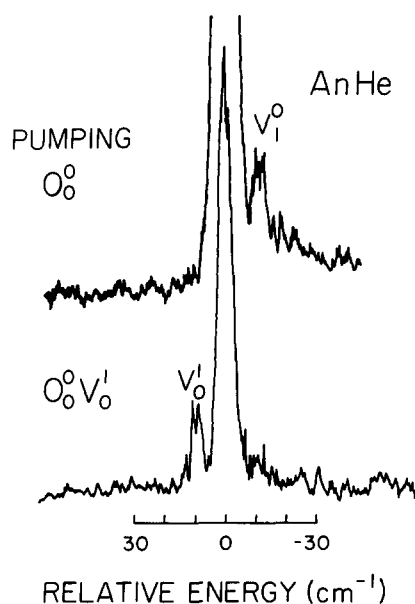


FIG. 3. One of the DE peaks obtained by pumping $\text{AnHe} 0_0^0$ (upper trace) and one quantum of the AnHe stretch. An was expanded with pure He at $P_0 = 600$ psi. The frequency scale is relative to $\text{AnHe} 0_0^0$. For these spectra, the slits are reduced to 5 cm^{-1} resolution. These spectra confirm the assignments of the absorption features being pumped.

and one member in the progression $I_2^0 V_x^0$ is clearly identified. If one quantum of the vdW stretch is excited, the progression $I_2^0 V_x^1$ is observed with the most prominent feature being $I_2^0 V_1^1$ indicating a strong $\Delta V = 0$ propensity rule. The observation that V^1 is nearly identical to V_1 (10.4 and 9 cm^{-1} , respectively) implies that $I_2^0 V_1^1$ is nearly isoenergetic with I_2^0 and indicates that the vdW potential is not essentially different in the ground and excited states.

It is proposed in I that relaxed emission observed while pumping An absorption peaks is actually due to vibrational predissociation of AnHe_x . Figure 4 presents strong additional evidence supporting this proposed

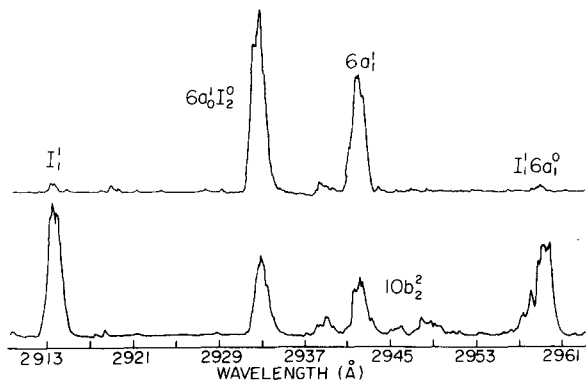


FIG. 4. DE spectra of $\text{An} 6a_1^0$. The upper trace is obtained from An-He with 0.2% CH_4 expanded at $P_0 = 500$ psi. The lower spectrum was obtained from An expanded with pure He at $P_0 = 600$ psi. Notice the dramatic decrease in the relaxed peaks, particularly I_1^1 and $I_1^1 6a_1^0$ due to the addition of CH_4 .

mechanism. The lower trace shows a portion of the DE spectrum obtained while pumping $An\ 6a_0^1$. The upper trace shows the same spectrum after a small amount of CH_4 has been mixed into the system. Note the dramatic decrease in the relative intensity of the relaxed peaks upon addition of CH_4 . Methane competes with He in the formation of vdW complexes. Addition of methane decreases the concentration of $AnHe_x$, as can be seen in the FE and mass spectra of this mixture, and thus reduces the apparent relaxation in the system. Further discussion of the implications of these data for the relaxation mechanisms previously proposed will be presented in the Discussion section.

B. An- CH_4 system

1. 0_0^0

This transition was studied most extensively because little interference exists in this case from other observable An bands. The well studied hot bands⁸ in this region disappear at $P_0 \gtrsim 250$ psi. $AnHe_x$ features are greatly reduced due to the presence of CH_4 , and the $AnHe_x$ absorption features are confined to the region immediately surrounding and to the blue of the $An\ 0_0^0$. Therefore, the observed absorption features in this region are due to $An(CH_4)_x$ species. No species of the form $An(CH_4)_xHe_x$ have been observed.

The region from 0 to $-80\ cm^{-1}$ relative to $An\ 0_0^0$ is dominated by the $AnCH_4$ species as is clearly shown in Fig. 5. The major features in the FE spectrum (upper trace) are reproduced in the two-color MS of $AnCH_4$. The spectrum consists of transitions due to the $AnCH_4\ 0_0^0$ $80\ cm^{-1}$ red shifted from the $An\ 0_0^0$ and various vdW motions of the $AnCH_4$ species to the blue of the $AnCH_4\ 0_0^0$ (see Table II). The $AnCH_4$ origin consists of three peaks: this triplet structure may arise from three slightly different conformations for the $AnCH_4$ species, or from vdW bending modes built on the $AnCH_4\ 0_0^0$. The relative intensities of the three peaks remain the constant as the nozzle backing pressure is varied, thus

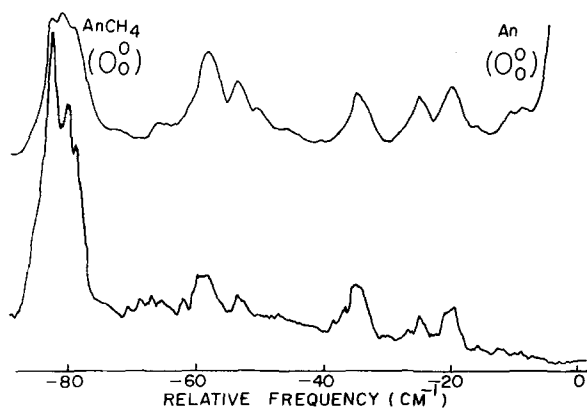


FIG. 5. FE (upper trace) and two-color MS of An-He and 0.1% CH_4 expansion at $P_0 = 500$ psi. The frequency scale is relative to $An\ 0_0^0$ at $34\ 031\ cm^{-1}$. The two-color MS experiment involves gating on the $AnCH_4$ mass channel. Note that the $AnCH_4$ two-color experiment reproduces all of the important features in the FE spectrum. The ionization frequency is $28\ 169\ cm^{-1}$.

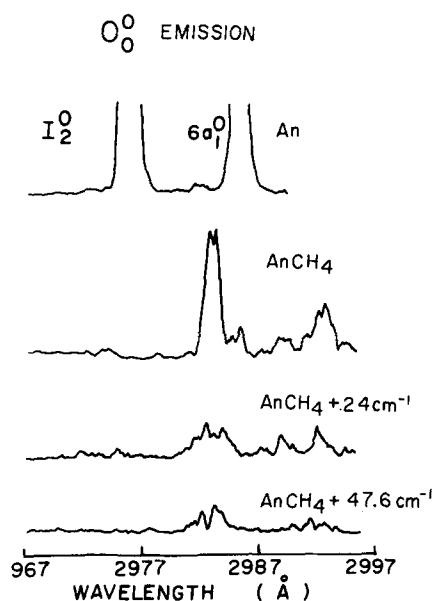


FIG. 6. Part of the DE spectra of $An\ 0_0^0$, $AnCH_4\ 0_0^0$, and two vdW vibrational peaks built on $AnCH_4\ 0_0^0$. An-He was expanded with 0.1% CH_4 at $P_0 = 500$ psi. Note that the major features of the $AnCH_4$ spectra are identical and red shifted by $\sim 80\ cm^{-1}$ relative to $An\ 0_0^0$.

eliminating hot bands and rotational structure as possible sources of the features.

The general assignment of the $AnCH_4\ 0_0^0$ region is supported by the DE spectra. Figure 6 shows a portion of the $An\ 0_0^0$ DE spectrum and the DE spectra of various $AnCH_4$ features. For all of the $AnCH_4$ features pumped the dominant emission is isoenergetic with emission from $AnCH_4\ 0_0^0$. Apparently, pumping a vdW motion of the $AnCH_4$ results in emission predominately to the same vdW motion in the ground state. This interpretation is supported by high resolution DE spectra. Figure 7 presents a small portion of the dispersed emission spectrum associated with pumping the origin region of

TABLE II. $An(CH_4)_x\ 0_0^0$ and $6a_0^1$ features from two-color MS experiments (see Figs. 5 and 12) ($An\ 0_0^0$ at $34\ 031\ cm^{-1}$ and $An\ 6a_0^1$ at $34\ 523\ cm^{-1}$).

Feature	$An(CH_4)_x\ 0_0^0$ (cm^{-1})	$An(CH_4)_x\ 6a_0^1$ (cm^{-1})	$An(CH_4)_2\ 0_0^0$ (cm^{-1})
V_0^0 (cm^{-1} relative to An)	0(-80)	0(-80)	0(-160)
vdW vibrations	9.7	10.5	
	16.9	17.4	
	24	24	
	28.5	29	
	31.7	32.4	
	36.6	37.4	
	47.6	47.6	
	56.7	57.1	
	61.7	61.9	
	65.7	66.2	
	71	70.7	
	72.7	72.5	

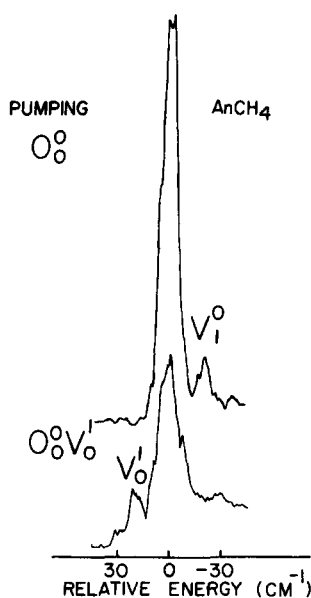


FIG. 7. High resolution spectra of the I_2^0 peak in the DE spectrum of AnCH_4 0_0^0 (upper trace), and an AnCH_4 vdW stretching motion. An was expanded in He with 0.1% CH_4 at $P_0=500$ psi. Spectral resolution is slit width limited at 10 cm^{-1} . These spectra identify the emitting levels and give the stretching frequency in the ground state as $\sim 25\text{ cm}^{-1}$.

AnCH_4 . If the AnCH_4 0_0^0 state is excited, emission is observed corresponding to the $I_2^0V_0^0$ and $I_2^0V_1^0$ transitions: if the AnCH_4 $0^0V_1^0$ state is excited, emission is observed corresponding to the $I_2^0V_1^1$ and $I_2^0V_0^1$ transitions. The relative intensities in the spectra further confirm the $\Delta V=0$ propensity rule previously suggested. These spectra not only support the assignment of the AnCH_4 0_0^0 features, but also show that the feature 24 cm^{-1} blue shifted with respect to the $\text{An}(\text{CH}_4)$ origin is one quantum of an AnCH_4 vdW motion. In addition, the observation that this motion is nearly the same in the ground and excited state (25 and 24 cm^{-1} , respectively) indicates

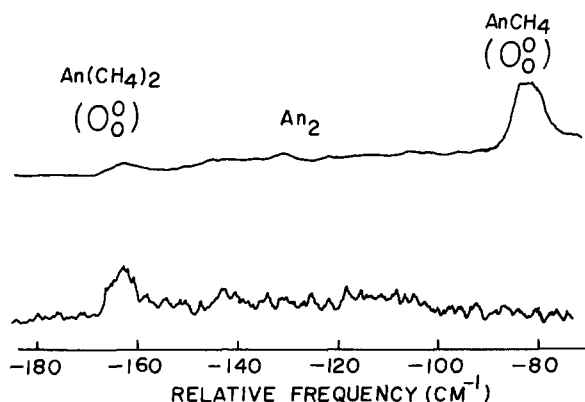


FIG. 8. FE spectrum of An expanded in He with 0.2% CH_4 at $P_0=400$ psi (upper trace) and two-color $\text{An}(\text{CH}_4)_2$ spectrum of An in He and 1.1% CH_4 at $P_0=400$ psi. Frequency scale is relative to $\text{An } 0_0^0$. Note that the FE spectrum is nearly identical to the two-color $\text{An}(\text{CH}_3)_2$ MS data except for the peak at -130 cm^{-1} which is assigned to An_2 .

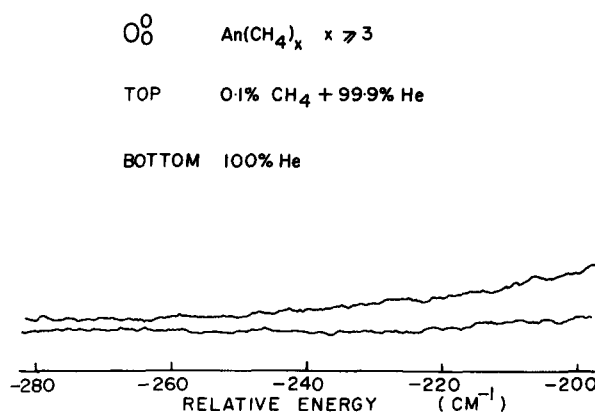


FIG. 9. FE spectra of An in He with 0.1% CH_4 at $P_0=800$ psi (upper trace), and An in pure He at $P_0=800$ psi. Frequency scale is relative to $\text{An } 0_0^0$. Note the gentle rise in the upper spectrum relative to the An-He base line. This is due to $\text{An}(\text{CH}_4)_x$, where $x > 3$.

that $\text{An}-\text{CH}_4$ potential surfaces do not differ greatly in the ground and excited states.

The spectral region from -80 to -160 cm^{-1} relative to the $\text{An } 0_0^0$ is dominated by the $\text{An}(\text{CH}_4)_2$ species as Fig. 8 indicates. The major features in the FE spectrum in this region (upper trace) are reproduced by two-color MS obtained by selective observation of the $\text{An}(\text{CH}_4)_2$ mass channel. The $\text{An}(\text{CH}_4)_2$ 0_0^0 is red shifted 162 cm^{-1} from the $\text{An } 0_0^0$ and some structure due to vdW bond modes is evident to the blue of the $\text{An}(\text{CH}_4)_2$ origin. The exception to this assignment is the band at -130 cm^{-1} in the FE spectrum. This feature is not a hot band as it increases rather than decreases with increasing nozzle backing pressure. It is not due to $\text{An}(\text{CH}_4)_2$ since it does not appear in the two-color MS; it has been assigned to the An_2 species although the appropriate two-color MS study to confirm this was inconclusive due to poor An_2 signal levels.

The FE spectrum to lower energy than the $\text{An}(\text{CH}_4)_2$ origin consists of a broad continuum that decreases in intensity to lower energy. Figure 9 shows that $\text{An}(\text{CH}_4)_x$ species generate a rising intensity background relative to An expanded in pure He. Mass spectra generated by excitation in this region, one of which is shown in Fig. 10, indicate that the absorption intensity in this region is dominated by the $\text{An}(\text{CH}_4)_3$ and $\text{An}(\text{CH}_4)_4$ species. This indicates that the spectral shifts of the origins of various clusters is no longer additive for $\text{An}(\text{CH}_4)_x$ with $x > 3$. The mass spectrum presented in Fig. 10 is obtained by one-color, two-photon ionization; the intensity in the An, $\text{An}(\text{CH}_4)$, and $\text{An}(\text{CH}_4)_2$ mass channels is due to fragmentation. Higher clusters are also observed in this mass spectrum indicating that they too absorb $\sim 200\text{ cm}^{-1}$ below the $\text{An } 0_0^0$ transition.

2. $10b_0^2$, $16a_0^2$

Figure 11 shows the FE and two-color MS of AnCH_4 associated with the $10b_0^2$ and $16a_0^2$ transitions. The spectral features differ significantly in relative inten-

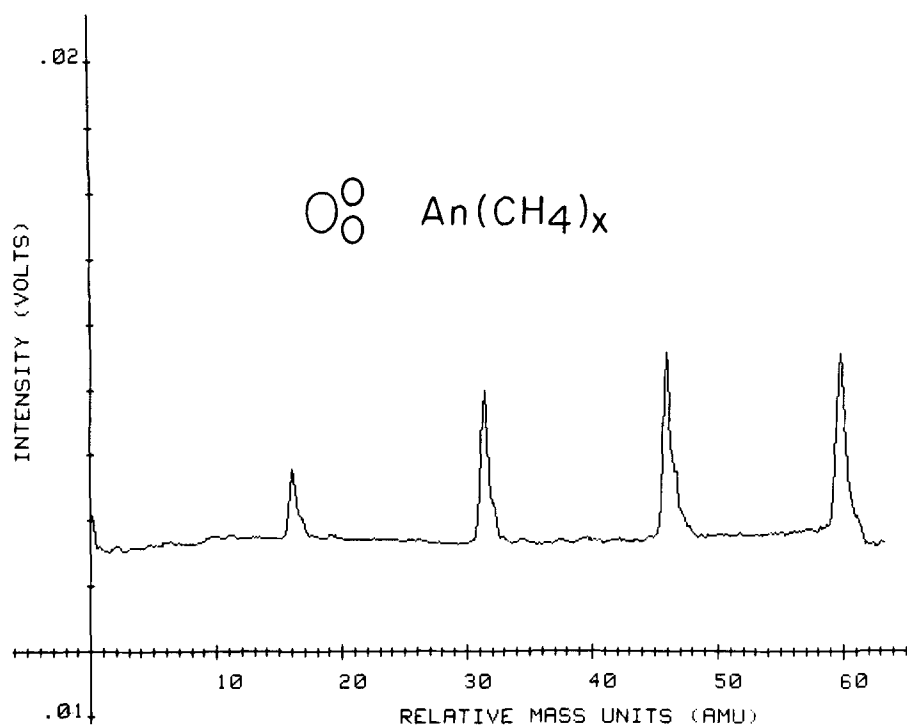


FIG. 10. One-color MS of An in He with 1% CH₄ at $P_0 = 800$ psi. The laser wavelength is 2960 Å which corresponds to the region in which An(CH₄)_x ($x \geq 3$) absorb. Mass units are relative to An. Notice that An(CH₄)₃ and An(CH₄)₄ dominate this region. Although not shown in this figure, An(CH₄)_x, species up to $x = 15$ are observed. Peaks corresponding to An(CH₄)_x, where $x \leq 2$ are due to fragmentation of larger clusters.

sities from those observed for the 0_0^0 transition. This is most likely due to the overlap of AnCH₄ features associated with $10b^2$ and $16a^2$ as these two levels are separated by only 8 cm⁻¹. Thus, the resulting spectra appear broad. Moreover, spectral intensity due to An(CH₄)₂ associated with the $6a_0^1$ transition further hampers a detailed study of the features related to An-CH₄ vdW clusters at $10b^2$ and $16a^2$.

3. $6a_0^1$

Figure 12 presented the FE and two-color mass spectra of AnCH₄ associated with the An $6a_0^1$ transition. The spectra of AnCH₄ for this transition are virtually

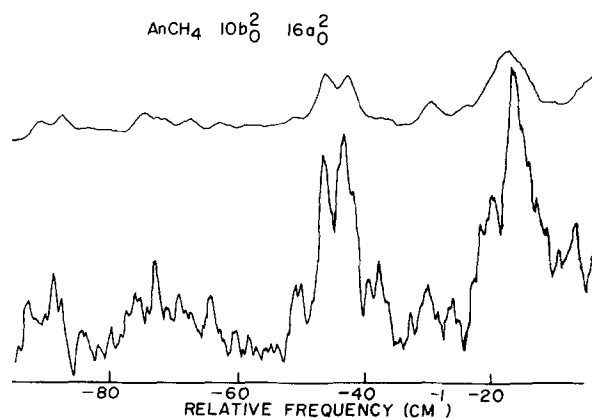


FIG. 11. FE spectrum near $10b_0^2$ of An in He with 0.2% CH₄ at 400 psi (upper trace) and two-color MS of AnCH₄ in the $10b_0^2$ region of An in He with 0.1% CH₄ at $P_0 = 500$ psi ($\nu_{\text{cm}^{-1}} = 28\,219$ cm⁻¹). Frequency scale is relative to An $10b_0^2$ (34 379 cm⁻¹). Note that this region is highly congested with peaks from $10b_0^2$, $16a_0^2$, and An(CH₄)₂ $6a_0^1$.

identical to those observed for the 0_0^0 transition with respect to relative intensities and shifts. Notice again the good correlation between the FE spectrum and the two-color MS. The -80 cm⁻¹ band is the most intense feature in both spectra and is thus assigned as the AnCH₄ $6a_0^1$ and the blue shifted bands relative to AnCH₄ $6a_0^1$ are its associated vdW modes. The relative energies

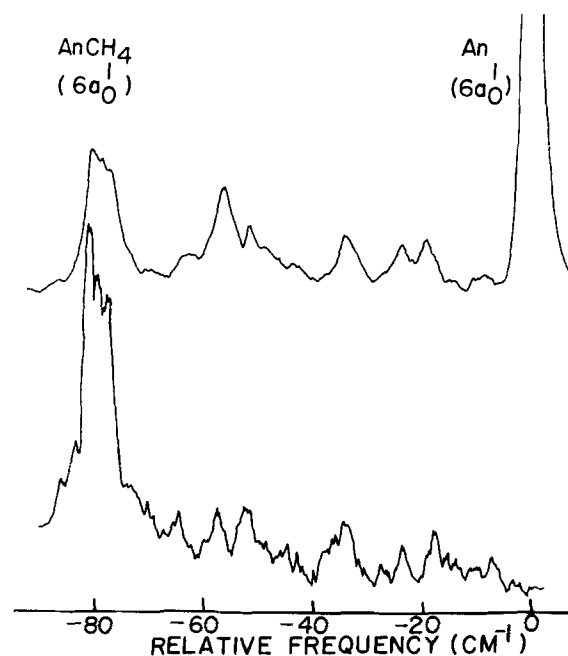


FIG. 12. FE spectrum of An in He with 0.2% CH₄ at $P_0 = 500$ psi near the An $6a_0^1$ transition (upper trace) and two-color MS of AnCH₄ for An in He with 0.1% CH₄ at $P_0 = 500$ psi and $\nu_r = 28\,219$ cm⁻¹. Frequency scale is relative to An $6a_0^1$ (34 523 cm⁻¹). Notice that the FE spectrum in this region is due largely to AnCH₄.

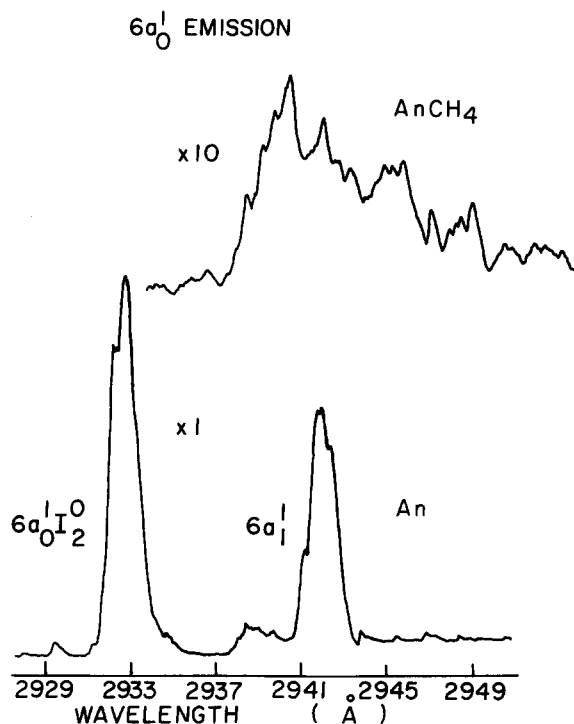


FIG. 13. DE spectrum of AnCH_4 $6a_0^1$ (upper trace) and DE spectrum of An $6a_0^1$. Both are obtained for An in He with 0.2% CH_4 at $P_0 = 500$ psi. Note that AnCH_4 $6a_0^1$ emission is broad and featureless and red shifted about 80 cm^{-1} from the An emission.

of various bands are tabulated in Table II.

Presumably, the $\text{An}(\text{CH}_4)_2$ $6a_0^1$ is red shifted 160 cm^{-1} from An $6a_0^1$ as is the case for this species near the origin transition. However, this feature would be buried in the congestion associated with the $10b_0^2$ and $16a_0^2$ transitions and could not be unambiguously assigned.

The DE spectrum of AnCH_4 associated with the $6a_0^1$ state shows broad features with high background. The estimated intensity of the emission features is at least five times weaker than expected. It should be empha-

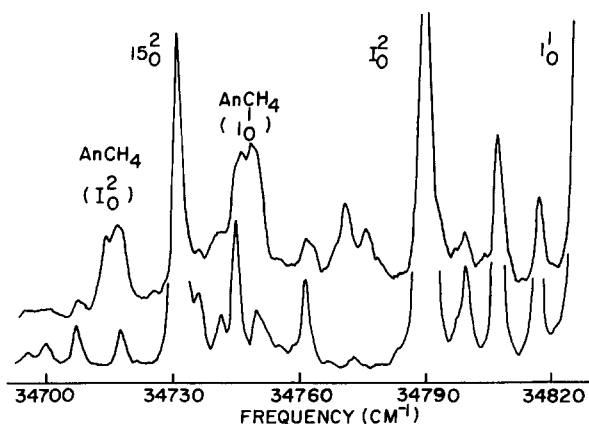


FIG. 14. FE spectrum near An 15_0^2 of An in He with 0.1% CH_4 at $P_0 = 600$ psi (upper trace) and An expanded in pure He at $P_0 = 600$ psi. Although the spectra are complicated by congestion, some AnCH_4 peaks are discernible.

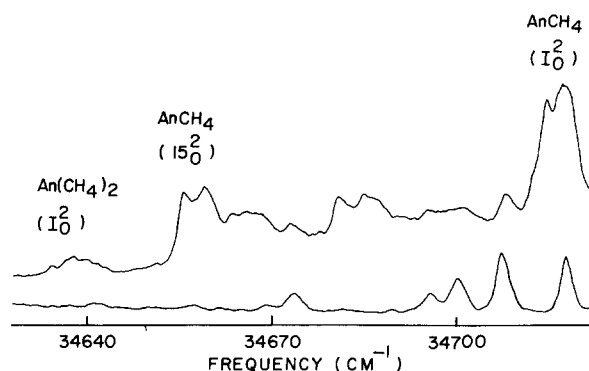


FIG. 15. FE spectra $10\text{--}90\text{ cm}^{-1}$ to the red of An 15_0^2 for An in He with 0.1% CH_4 (upper trace) and An in pure He , both at $P_0 = 600$ psi. Several AnCH_4 bands are identifiable.

sized that the DE spectrum of the An monomer of this transition shows no broadening. Figure 13 presents a portion of the DE spectra generated by pumping An $6a_0^1$ (lower trace) and $\text{An}(\text{CH}_4)$ $6a_0^1$. This broadening is most likely due to IVR, as will be discussed more fully in the next section.

4. Higher vibronic transitions

Figures 14, 15, and 16 show FE spectra of the $\text{An}\text{--}\text{CH}_4$ system (upper traces) compared to some spectra with $\text{An}\text{--}\text{He}$ only. Although this region is highly congested, careful examination of the spectra reveals absorption features due to $\text{An}(\text{CH}_4)_x$. Transitions 15_0^2 , I_0^1 , and I_0^2 of AnCH_4 can be distinguished and their spectral red shifts from their An counterparts are 75, 77, and 82 cm^{-1} , respectively. The 15_0^2 and I_0^2 transitions of $\text{An}(\text{CH}_4)_2$ can also be identified with red shifts of 152 and 153 cm^{-1} , respectively. No two-color MS are observed in this region due to vibrational predissociation (VP) of the vdW species. Dispersed emission from the AnCH_4 15_0^2 (Fig. 17) shows sharp features from the An 0^0 level only, thus confirming that the AnCH_4 15^2 level undergoes rapid VP. Emission from I^2 and I^1 levels evidenced similar results.

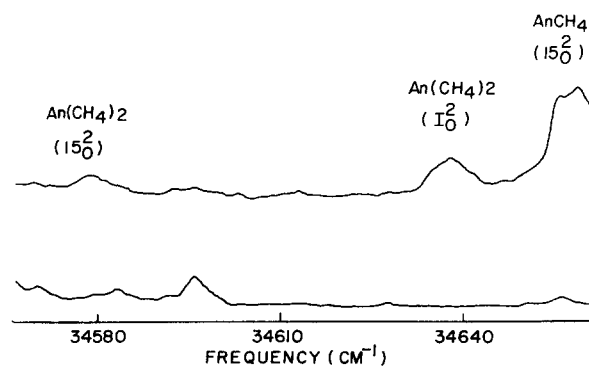


FIG. 16. FE spectra $80\text{--}160\text{ cm}^{-1}$ to the red of An 15_0^1 for An in He with 0.3% CH_4 (upper trace) and An in pure He , both at $P_0 = 300$ psi. Several $\text{An}(\text{CH}_4)_2$ features can be identified.

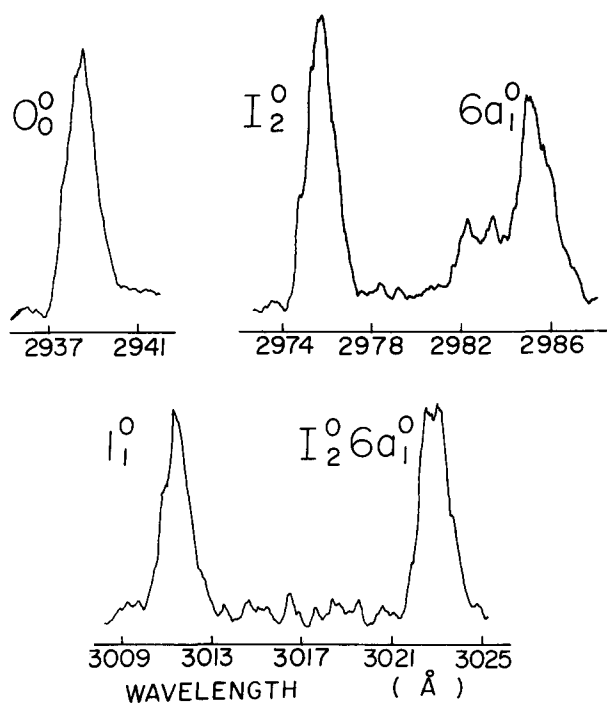


FIG. 17. Portions of the DE spectrum of AnCH_4 15%. An was expanded in He with 0.1% CH_4 at $P_0 = 600$ psi. The observed AnCH_4 15% emission is identical to $\text{An } 0_0^0$ emission indicating complete and rapid VP at 15% of AnCH_4 .

IV. DISCUSSION

In this section, discussions will focus both on the physical properties of the clusters and on the relaxation mechanisms of the excited species. The An-He system will be discussed first, followed by the An- CH_4 system.

A. An-He system

Two central questions concerning the physical properties of AnHe complexes remain unanswered in the discussion of the An-He system in I: what is the dissociation energy (D_0) of the An-He complex, and what are the geometries of these complexes? The two-color MS experiment has made it possible to obtain distinct and identifiable absorption spectra of each AnHe_x species individually in the 0_0^0 region (Fig. 2). These spectra, together with the high resolution DE spectra (Fig. 3), have led to an unambiguous assignment of the FE spectra and have shed some light on the questions concerning D_0 and geometry.

The dissociation energy of the AnHe complex can be estimated from the vdW stretch progression observed in the two-color MS spectrum (Fig. 2). The calculation using this progression and assuming a Morse potential gives a value for D_0 of about 100 cm^{-1} . It is not possible to use two-color TOFMS to estimate the binding energy for An-He clusters because vibronic transitions within 200 cm^{-1} of the An origin are not observed. As will be discussed below however, DE spectra can be analyzed to bracket the binding energy.

In paper I, several mechanisms were proposed which

could lead to the fluorescence observed upon exciting a vdW feature. As was suggested previously and is stated more definitively below, an excited AnHe_x can evidence two relaxation pathways under the conditions in the beam: fluorescence to the ground state (SVLF), predominantly to levels with the same quanta of the vdW stretching vibration as in the excited state, or vibrational predissociation (VP) followed by monomer An fluorescence. Assuming that only these two mechanisms are important under our experimental conditions, it is possible to re-examine some of the DE data and get a better estimate of D_0 . The lower trace of Fig. 4 shows part of the DE spectrum obtained by pumping An $6a_0^1$ (and necessarily $\text{AnHe } 6a_0^1$ and $\text{AnHe}_2 6a_0^1$). Several relaxation peaks are evident in this spectrum, most notably I_1^1 and $I_1^1 6a_1^0$: these peaks are due to VP of AnHe and AnHe_2 . Since the difference in energy between the $6a^1$ and I^1 levels in An is 155 cm^{-1} , D_0 for AnHe (the dominate vdW species) must be less than 155 cm^{-1} .

With the help of additional assumptions, further examination of the $6a_0^1$ DE spectrum can also yield an estimate of the lower limit of D_0 . A small emission peak in this spectrum, identifiable as $10b_2^2$, is observable, although it is much weaker than I_1^1 . One possible explanation for the poor intensity of $10b_2^2$ is that the oscillator strength of the transition is much smaller than for I_1^1 . However, DE spectra from $10b^2$ presented in I show the $10b_2^2$ peak to be quite strong. The only direct comparison of I_1^1 and $10b_2^2$ intensity is found in the I_1^0 DE spectrum,⁶ for which both the I_1^1 and $10b_2^2$ peaks, arising from $\text{An}(\text{He})_x$ VP, are very weak due to the large difference in energy between I^1 and $10b^2$ and the much higher I^1 level. Nevertheless, considering the data in I it would seem safe to assume that the oscillator strengths of I_1^1 and $10b_2^2$ are comparable (within a factor of ~ 2).

Assuming that I_1^1 and $10b_2^2$ have comparable oscillator strengths, the only explanation for the small intensity of the $10b_2^2$ transition in the $6a_0^1$ spectrum is that the energy gap between $6a^1$ and $10b^2$ is not sufficient to break the AnHe bond. This leads to a lower limit for D_0 of 144 cm^{-1} .

If AnHe were the only vdW species in the beam and the An-He $D_0 = 150 \text{ cm}^{-1}$, one would predict no intensity for the $10b_2^2$ transition in the $\text{AnHe } 6a_0^1$ DE spectrum. However, several situations could produce a small amount of intensity for $10b_2^2$ in our system. One explanation for this intensity is that D_0 for the first He from AnHe_x ($x \geq 2$) is less than 144 cm^{-1} . Since the concentration of AnHe_x is much less than AnHe, the AnHe_x VP peaks would be of much less intensity than those due to VP of AnHe. Another explanation is that the AnHe D_0 is very close to 144 cm^{-1} and some VP to $10b^2$ is seen due to the contribution of a small amount of rotational energy. Finally, AnHe may undergo IVR as the An- CH_4 system can. One would expect such emission to be weak and broad. All of these explanations for the observed $10b_2^2$ intensity are consistent with $D_0 > 144 \text{ cm}^{-1}$ for AnHe.

It is not possible to arrive at a definitive description of the geometry of the An-He vdW species without

higher resolution spectra which show resolved rotational structure. However, some geometry information can be gleaned from the existing data. The two-color MS (Fig. 2) show a nearly additive spectral red shift for the AnHe_0^0 and AnHe_2^0 peaks. This probably indicates that the He atoms are adding to two nearly equivalent positions on the An. It is easy to envision only one way to put two and only two equivalent He atoms on An; they must occupy the positions above and below the aromatic ring in a manner analogous to that suggested for tetrazine-He vdW species.⁹ This is consistent with the observed red shift of the clusters. He atoms above and below the ring should be more tightly bound in the excited state than in the ground state of An.

The addition of a third He to produce a broad absorption spectrum with a nonadditive shift is consistent with the addition of the He to a nonlocalized, nonring position, perhaps near the NH_2 group. Larger clusters (AnHe_x , $x > 3$) are also observed by one-color MS to absorb in the same region as the AnHe_3 clusters. The absorption profile for a system of AnHe_x in which $x \geq 3$, with its limiting value of solvent shift, begins to resemble that of a solution.

Several questions concerning the possible pathways which an excited AnHe_x can take were raised previously in I. The conclusions reached in that work, some of which were tentative, were as follows: an An^* molecule can only fluoresce from the vibronic level that was excited (SVLF); an AnHe_x^* can fluoresce to levels in the ground state with the same quanta of vdW vibrations as in the excited state (SVLF, $\Delta V = 0$); and an AnHe_x^* can VP generating An^* which can fluoresce from a level lower than the one pumped. Mechanisms involving collisions were effectively ruled out as significantly contributing to the relaxation for the beam conditions in our system.

Information presented in this paper strengthens these conclusions. Collisions are further shown not to be important under these beam conditions by the data presented in Fig. 4. Addition of CH_4 is observed to reduce the concentration of AnHe_x species and $\text{An}(\text{CH}_4)_x$ species do not yield relaxed An emission when An absorption bands are excited. Since reducing the AnHe_x concentration reduces the relaxation, it follows that the relaxation seen when An absorption bands are excited (as well as underlying AnHe_x absorption bands) is associated with VP of the AnHe_x species.

Among other mechanisms, the SVLF of AnHe_x species with a $\Delta V = 0$ propensity rule was proposed to explain the monomer-like emission found by exciting AnHe_x absorption features around the $\text{An } 0_0^0$ transition. Figure 3 demonstrates that AnHe_x species in this region are indeed emitting to produce predominantly monomer-like emission. Furthermore, the lower trace in Fig. 3 emphasizes that if vdW stretches are excited, the fluorescence obeys a $\Delta V = 0$ propensity rule. This information, plus the deduced D_0 , indicates that only SVLF with $\Delta V = 0$ is occurring to any great extent from vibronic levels of AnHe_x with insufficient vibrational energy to undergo VP.

B. An- CH_4 system

The principle observations for the An-He system are applicable to the An- CH_4 system with some modification. The internal modes of An show little, if any, change in the CH_4 cluster. The AnCH_4^0 and $\text{An}(\text{CH}_4)_2^0$ have additive spectral red shifts relative to the $\text{An } 0_0^0$, although the shifts are much greater than for AnHe_x due to the larger polarizability of CH_4 . Addition of a third CH_4 produces broad, featureless absorption indicating that, while the first two CH_4 groups add to equivalent positions on the An (above and below the aromatic ring) the third CH_4 adds to an inequivalent, less localized position. These observations are qualitatively similar to those made for the An-He system.

Perhaps the most striking difference between the An- CH_4 and An-He systems is the observation of extensive IVR in the An- CH_4 system. This process will be discussed in detail following a discussion of the physical properties of the An- CH_4 clusters.

The general appearance of the An- CH_4 absorption spectra evidences much more congestion than is observed in the An-He spectra. The possible appearance of three conformers each with a different stretching mode, plus the possibility that bending modes may be contributing intensity, can account for the congestion. The congestion increases as more CH_4 molecules are added to the cluster. For three or more CH_4 solvent molecules coordinated to an An solute, the spectrum transforms into a broad structureless feature whose center is to the low energy side of the $\text{An}(\text{CH}_4)_2^0$. In both shape and position, such a feature for $\text{An}(\text{CH}_4)_x$ ($x \geq 3$) is quite similar to the liquid solution state spectrum of aniline. Cryogenic solution spectra of An- CH_4 were not obtainable due to low solubility; however, one can predict by comparison with benzene and toluene solution data that an An- CH_4 solution would give an $\text{An } 0_0^0$ red shift of $\sim 250 \text{ cm}^{-1}$.¹⁰

Higher transitions exhibit similar spectral shifts and patterns in the vdW vibrations. These absorption patterns are identifiable in the $\text{AnCH}_4 6a_0^1$ region (Fig. 12) for which they are free of congestion from other vibronic bands. The emission spectra of higher vibronic bands can give an estimate of the dissociation energy of the AnCH_4 complex. Emission from $\text{AnCH}_4 15^2$ or higher levels evidence strong, sharp emission from the $\text{An } 0^0$ level as given in Fig. 17. This demonstrates that 699 cm^{-1} is sufficient to cause VP of the An- CH_4 bond and sets a firm upper limit to the dissociation energy.

Emission from the $\text{AnCH}_4 6a^1$ level is broad and featureless and shifted $\sim 80 \text{ cm}^{-1}$ to the red of $\text{An } 6a^1$ emission. Time-of-flight mass spectra taken with $6a^1$ as the intermediate level demonstrate that excitation to the $\text{AnCH}_4 6a^1$ level does not lead to VP and therefore $D_0 > 498 \text{ cm}^{-1}$. The emission from $\text{AnCH}_4 10b^2$ and $16a^2$ is similar in appearance although much weaker than the $\text{AnCH}_4 6a^1$ emission as is expected.

The broad and featureless appearance of the $\text{AnCH}_4 6a_0^1$ emission (Fig. 13) is attributed to IVR of the $\text{AnCH}_4 6a^1$ level before emission. The IVR process may arise

in the An-CH₄ system and not in the An monomer due to the increased density of states afforded by the creation of various vdW modes. The largest features in the AnCH₄ 6a₀¹ emission spectrum are red shifted ~80 cm⁻¹ from the An 6a₀¹ spectrum. However, near the AnCH₄ 6a₀¹I₂⁰ emission peak (Fig. 13), for example, substantial intensity is present to the red of the major peak. This intensity may be due to IVR generated features such as 10b₁¹, 10b₂², and 15₁¹, or it could be due to emission from several vdW modes built on different An vibronic levels populated by the IVR process. In any case, the general appearance of the spectrum leads to the conclusion that IVR is important at the AnCH₄ 6a₀¹ level, although some SVLF may be found within the IVR related emission background.

Although it is impossible to set quantitative rates for the IVR or VP processes from the observed spectra, it is possible to compare qualitatively the rates for IVR and VP with the fluorescence rate. The rate of VP is fast compared to the fluorescence lifetime (5 ns) since the VP process is complete within this period. Also, an upper limit to the rate of VP can be estimated from the linewidth of the transitions to states more than 699 cm⁻¹ above CH₄ 0₀⁰. Since the linewidths do not change noticeably between transitions to states that undergo VP and those that do not, the lines are inhomogeneously broadened and the rate of VP must be much slower than the linewidth estimated lifetime of 5 ps would indicate. The rate of IVR must be much slower than the rate of VP since the DE from AnCH₄ 15² and higher level does not evidence any IVR related broad emission. It can also be concluded that the rate of IVR is somewhat faster than the rate of fluorescence since the AnCH₄ 6a₀¹ emission does not show strong SVLF, although IVR is not a great deal faster than the fluorescence rate since IVR is not complete before the complex fluoresces. One can, therefore, express qualitatively the relative rates as follows: fluorescence (10⁹/s) < IVR << VP << 10¹²/s.

Relaxation rates in collisionless environments have been studied in other systems.¹¹ In the tetrazine-argon (Tet-Ar) system¹² the rate of IVR is comparable to the rate of VP. Pumping an excited vibronic level results in SVLF, sharp, relaxed emission due to VP, and broad, symmetric emission peaks due to IVR. The fluorescence intensity associated with each of these processes is compared to find the relative rates for the different processes. In the Tet-Ar system, the SVLF rate is fastest, with the IVR and VP rates nearly the same for many levels. It appears that the rate of IVR for a system is primarily governed by the density of states in the system.

In light of the above discussion concerning the IVR process in An-CH₄ clusters, it is possible to draw another parallel between vdW clusters and liquid state behavior. For liquids, in general, what emission does occur almost invariably arises from the lowest vibrational level of the first excited state of a given spin manifold.¹³ Moreover, the emission from liquids tends to be broad and is often temperature dependent. Most of these trends are distinctly seen in An(CH₄)_x vdW clusters. As cluster binding energy becomes larger

(better solvents) and presumably as cluster size increases, IVR becomes a more dominant process. As IVR becomes faster, thermal equilibrium can be established more readily in the excited state for both clusters and real solutions. Indeed, the excited state kinetics observed in the liquid can be explained by a rapid IVR process which arises, not from a perturbation of solute levels *per se*, but from a substantial increase in the density of states experienced by the solute and associated with local solute/solvent clusters or solvent cage formation. In solution, such clusters are necessarily of a highly dynamic nature but they may live for a time long compared to the cluster VP and IVR times.

V. CONCLUSIONS

The two-color MS technique has allowed a much greater understanding of both the physical properties and the relaxation processes in the An-He and An-CH₄ systems. The essential general conclusions which follow for the vdW cluster systems are enumerated below.

- (1) The AnHe 0₀⁰ and AnHe₂ 0₀⁰ evidence additive red shifts relative to An 0₀⁰, whereas the AnHe₃ 0₀⁰ is broad and exhibits a nonadditive spectral shift. Larger clusters (x > 3) absorb in the region of AnHe₃ indicating a limiting value for a cluster (solvation or cage) shift.
- (2) Both An-He and An-CH₄ vdW species seem to show a strong preference for binding the ligand above and below the An aromatic ring.
- (3) An-He vdW stretching modes are clearly evident and can be used to estimate the An-He dissociation energy as 100 ± 50 cm⁻¹. DE experiments can be used to bracket the dissociation energy at 144 cm⁻¹ < D₀ < 155 cm⁻¹.
- (4) Excited AnHe_x clusters undergo VP if sufficient vibrational energy is present, otherwise, they undergo SVLF with a strong ΔV = 0 propensity rule. Excited An can only exhibit SVLF under the experimental conditions of the present study.
- (5) AnCH₄ and An(CH₄)₂ vibronic bands show additive spectral red shifts of 80 and 160 cm⁻¹, respectively. The An(CH₄)₃ 0₀⁰ appears to be broad and apparently exhibits a nonadditive spectral shift. Larger clusters of An-CH₄ absorb in the same region as An(CH₄)₃, indicating that the limiting value for a cluster (solvation or cage) shift is produced by three solvent molecules for both He and CH₄.
- (6) The AnCH₄ 0₀⁰ and 6₀¹ are split into three peaks due to the presence of more than one conformer, or the presence of vdW bending modes or both.
- (7) The dissociation energy of AnCH₄ is between 498 and 699 cm⁻¹.
- (8) If AnCH₄ is excited with ≤ 498 cm⁻¹ of excess vibrational energy, the emission is broadened by IVR.
- (9) The rate of IVR from the AnCH₄ 6a₀¹ level is somewhat faster than fluorescence and substantially slower than the rate of VP.
- (10) The vdW potentials for both the An-He and

An-CH₄ systems are similar in the ground and excited states of a given species.

Some similarities can be pointed out between solution phenomena for molecules like An in simple cryogenic molecular hydrocarbon liquids and gas phase vdW clusters for the same solute/solvent sets. The two most striking similarities are the apparent importance of the IVR process for excited state kinetics in both clusters and solutions, and the limiting of the cluster (red) shift at roughly three solvent molecules at a value similar to the solution value.

Future studies are aimed at obtaining high resolution FE and two-color MS of the different clusters in order to gain more information about geometry; high resolution spectra may also be useful for a vibrational analysis of the vdW cluster modes. Other systems are being explored to answer questions about the IVR process, and to establish the relationship between the physical properties of vdW species and cryogenic solution spectra.

¹See, for example, D. H. Levy, L. Wharton, and R. E.

Smalley, *Chemical and Biochemical Applications of Lasers* (Academic, New York, 1977), Vol. II, pp. 1-41.

²See, for example, A. Amirav, U. Even, and J. Jortner, *J. Chem. Phys.* **75**, 2489 (1981).

³J. E. Kenny, K. E. Johnson, W. Sharfin, and D. H. Levy, *J. Chem. Phys.* **72**, 1109 (1980).

⁴J. H. Brophy and C. T. Rettner, *Chem. Phys. Lett.* **67**, 351 (1979).

⁵M. A. Duncan, T. G. Dietz, and R. E. Smalley, *J. Chem. Phys.* **75**, 2118 (1981).

⁶E. R. Bernstein, K. Law, and Mark Schauer, *J. Chem. Phys.* (in press).

⁷K. M. Swift, Ph.D. thesis, Colorado State University, 1981.

⁸J. C. D. Brand, D. R. Williams, and T. J. Cook, *J. Mol. Spectrosc.* **20**, 359 (1966).

⁹R. E. Smalley, L. Wharton, D. H. Levy, and D. W. Chandler, *J. Chem. Phys.* **68**, 2487 (1978).

¹⁰E. R. Bernstein, K. Law, and Mark Schauer (unpublished result).

¹¹(a) R. E. Smalley, *J. Phys. Chem.* **86**, 3504 (1982); (b) J. Langelaar, D. Babelaar, M. W. Leeuw, J. J. F. Ramaekers, and R. P. H. Ruttschnick, *Springer Series in Chemical Physics* (Springer, Berlin, 1980), Vol. 14, p. 171.

¹²D. V. Brumbaugh, J. E. Kenny, and D. H. Levy, *J. Chem. Phys.* **78**, 3415 (1983).

¹³F. Li, J. Lee, and E. R. Bernstein, *J. Phys. Chem.* **86**, 3606 (1982).